J Mater Sci (2006) 41:5061–5067
DOI 10.1007/s10853-006-0446-4

Ab initio modeling of clean and Y-doped grain boundaries in alumina and intergranular glassy films (IGF) in β-Si_3N_4

W. Y. Ching · Jun Chen · Paul Rulis · Lizhi Ouyang · Anil Misra

Received: 28 October 2005 / Accepted: 30 December 2005 / Published online: 18 July 2006

Abstract Based on large and relaxed grain boundary (GB) models in alumina and intergranular glassy film (IGF) models in polycrystalline β-Si_3N_4, ab initio modeling and theoretical tensile experiments were carried out for both clean and Y-doped models. It is shown that the increased covalent bonding between Y and O or N through the participation of the Y-4d and Y-3p orbitals is the mechanism by which Y ions enhance the mechanical and elastic properties of the Y-doped GB and IGF models. In alumina, this explains the improved creep behavior in the presence of Y doping. Preliminary results on the electronic structure and bonding of a specific GB model ($\Sigma 37$) in α-Al_2O_3 is presented. For the IGF models, the distribution patterns of Y ions in the glassy region were investigated by total energy calculations. Y ions prefer to be at the interfacial region between the IGF and bulk crystal. Defect-like states of different origin can be identified near the valence band and the conduction band edges. These theoretical predictions obtained from the calculation of the fundamental electronic structure of the materials can be used to derive local strain fields of dissimilar ''particles'' that may be linked to continuum level theories via finite element methods.

W. Y. Ching (✉) · J. Chen · P. Rulis · L. Ouyang
Department of Physics, University of Missouri-Kansas City, Kansas City, Missouri 64110, USA
e-mail: chingw@umkc.edu

J. Chen
Institute of Applied Physics and Computational Mathematics, Beijing 100088, China

L. Ouyang
Department of Mathematics and Physics, Tennessee State University, Nashville, Tennessee 37221, USA

A. Misra
Department of Civil and Mechanical Engineering, School of Computing and Engineering, University of Missouri-Kansas City, Kansas City, Missouri 64110, USA

Introduction

In recent years, computational materials science has made great strides in detailing many of the phenomena present in complex materials that were previously impossible to explain. Much of this success has been attributed to ever increasing computational power and improved methodologies to solve such problems in a realistic manner. Concerning polycrystalline structural ceramics and their interfaces, the presence of grain boundaries (GBs) and intergranular glassy films (IGFs) are well known because these microstructures dictate much of the mechanical and electronic properties of the bulk material. Their proper understanding and control is key to their successful application in emerging nanotechnology. Past theoretical studies of the microstructures in ceramics were mostly limited to crude empirical models or were based on simple idealized structures which rarely dealt with interactions at the atomistic level. For complex microstructures such as GBs and IGFs, it is necessary to first have realistic structural models and then to study their electronic structure, inter-atomic bonding, and charge distributions in order to reveal the microscopic origin of their useful properties at the nano- or bulk scale.

In this paper, we present some recent results from the computational modeling of GB models in alumina and IGF structures in β-Si_3N_4 based on large-scale first-principles calculations. Within the last few years, we have studied the structures and properties of several GB models in α-Al_2O_3 including the $\Sigma 3$ [1] and $\Sigma 31$ [2] models between basal planes of α-Al_2O_3 and a general $\Sigma 37$ GB [3]. For the IGF structure in β-Si_3N_4, a periodic model with 798 atoms with a 10 Å glassy region sandwiched between the crystalline [0001] planes was studied in considerable detail [4]. Both the clean structure and Y-doped structures were investigated [5]. It is shown that these results not only explain some of the existing experimental observations but can also predict certain behaviors or properties that are difficult to obtain other wise. We will highlight some of these results as examples. More importantly, we argue that such large-scale atomistic level calculations provide a pathway to bridge a gap in general multi-scale modeling by generating more reliable data for modeling materials at the mesoscopic or even macroscopic continuum level.

Methodology

For realistic calculations of microstructural models in ceramics at the ab initio level, a single computational method is usually not effective. We use two well-tested and extremely efficient computational methods based on density functional theory (DFT) [6, 7] for such calculations. The first one is a plane-wave based pseudo-potential method as implemented in the Vienna Ab initio Simulation Package (VASP) [8, 9]. In the VASP calculations, the PW-91 GGA potential for exchange-correlation potential was used with an energy cut-off of 400 eV. Because the supercells that represent the GB or the IGF models are fairly large, it is sufficient to use only one general k-point in the Brillouin zone. The structures were relaxed under the Hellmann–Feynman force with all atoms in the model relaxed to equilibrium positions such that the residual force on each atom is no larger than 0.01 eV/Å. It usually takes 25–30 iterations for the structure to converge to the desired level. These relaxed structures were then used to calculate the electronic structure and bonding using another ab initio method, the orthogonalized linear combination of atomic orbitals (OLCAO) method [10]. For the theoretical tensile ''experiments'', the ''samples'' were deformed by applying incremental stresses in the direction perpendicular to the GB line of the IGF layer until the samples were fully fractured. At each stress, the model was fully relaxed using VASP and the resulting strain evaluated. The stress versus strain relationship for the sample was thus obtained. The fracture energy of the GB or the IGF could then be obtained from the calculated total energies.

The second method, the OLCAO method, is also a DFT method using the local density approximation (LDA) in which the basis functions are expanded in terms of localized atomic orbitals [10]. The OLCAO method has been extensively used in the study of the electronic structure, bonding, and other physical properties of many crystalline and non-crystalline systems [1, 2, 4, 5, 11–19]. It is especially effective for highly complex structures where other ab initio methods may have some limitations. The use of atomic orbitals in the basis set enables us to analyze the results in a physically more intuitive way using the Mulliken population analysis scheme [20]. Quantitative results such as effective charges (Q^*) on each atom, the bond-order between any pair of atoms, charge density distributions, and atom-resolved partial density of states (PDOS) can be obtained. In the present 798 atom IGF model study the basis functions consist of the atomic orbitals of: Si (1s, 2s, 3s, 2p, 3p, 3d), O (1s, 2s, 2p), N (1s, 2s, 2p) and Y (1s, 2s, 3s, 4s, 5s, 2p, 3p, 4p, 5p, 3d, 4d). The dimensions of the secular equations to be diagonalized are 4,802 and 4,850 for the pure and Y-doped cases. In the OLCAO calculation, the entire spectrum of the energy eigenvalues and the wave functions are obtained.

Results and discussion

The $\Sigma 37$ grain boundary models in alumina

Grain boundaries in alumina have been extensively studied in recent years both experimentally [21–28] and theoretically [1, 3, 29–33]. Because of the constraint of periodic boundary conditions on these ab initio calculations, there are two oppositely directed grain boundaries in each model. A sufficiently large supercell is preferred to avoid any potential interactions between the two. Figure 1 shows the $(01\ \bar{1}8)/[04\ \bar{4}1]/180°$ ($\Sigma 37$) grain boundary model that has been relaxed using VASP for only 15 steps. The diffusion behavior of the ions in both the clean and Y-doped cases was recently studied using molecular dynamics [3]. This is a general grain boundary model with 280 atoms in the form of an elongated supercell with dimension of a = 41.5608 Å, b = 4.7142 Å, and c = 11.7325 Å. The calculated GB formation energy from the total energy difference between the $\Sigma 37$ model and the reference model of a

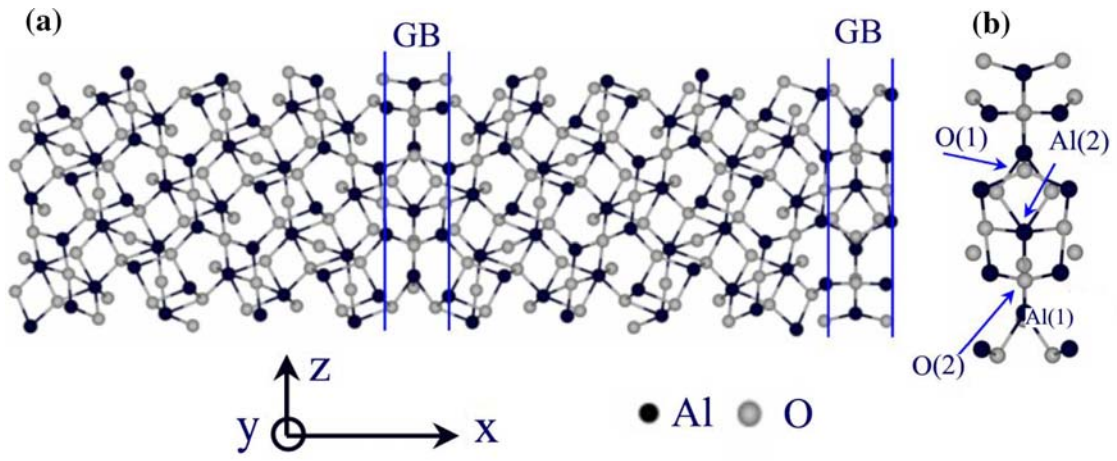

Fig. 1 The supercell model of the Σ37 GB in alumina

perfect crystal with the same number of atoms is 2.176 J/m^2. Here we report the results of the electronic structure and bonding calculated by the OLCAO method based on this preliminary model.

The Σ37 model is divided into GB regions of about 2.65 Å in width and the remaining bulk region as illustrated in Fig.1. Each GB region contains 12 Al atoms and 18 O atoms. These atoms can be further classified into two types each. There are four Al(1) atoms which are 5-fold bonded and eight Al(2) atoms that are 6-fold bonded. There are 6 (12) 3-fold (4-fold) bonded O atoms denoted as O(1) and O(2). Thus, the main characteristic of the Σ37 GB is the presence of the under-coordinated Al and O ions that result in large open spaces as shown in Fig. 1. The bond lengths (BL) of the GB atoms are listed in Table 1.

Figure 2 shows the calculated Mulliken effective charges Q^* for all the atoms in the Σ37 GB model. They range from 6.83 to 7.04 electrons for the O ions and from 1.49 to 1.77 electrons for the Al ions. In the bulk region, there is a small range of distributions for both cations and anions. In the GB region, the under coordinated Al(1) ions have, as expected, a slightly smaller Q^*. This slight change in Q^* could also be due to the changes in the Al–O BLs for atoms in the GB region as listed in Table 1.

The bond order (BO) values between the ions in the GB and the bulk region are calculated and listed in

Table 1 Calculated bond order (BO), bond length (BL) and effective charges Q^* for atoms in the bulk and GB region of the Σ37 GB model in α-Al_2O_3

BO (in elec.) (BL in Å) in the Σ37 GB model		
In the GB region		
Al (1)–O (1)	0.1856 (1.841); 0.2231 (1.927); 0.2014 (1.839)	
Al (1)–O (2)	0.2064 (1.835); 0.1961 (1.951); 0.1960 (1.954); 0.1828 (1.991); 0.1743; (1.797) 0.1630 (1.915)	
Al (2)–O (1)	0.1469 (1.931); 0.2231 (1.927); 0.1822 (1.962)	
Al (2)–O (2)	0.1554 (1.837); 0.2124 (1.849); 0.2251 (1.842); 0.2337 (1.824); 0.1809 (1.926); 0.1400 (1.948); 0.1686 (1.982)	
In the bulk region (averaged values)		
Al–O	0.1722 (1.906)	
BO (in elec.) (BL in Å) in perfect crystal α-Al_2O_3		
Al–O	0.1872 (1.857), 0.1436 (1.969)	
Mulliken effective charges Q^* in the Σ37 GB model (electrons)		
In GB region:	In the bulk region (averaged)	In perfect crystal α-Al_2O_3
Al(1) 1.574	Al 1.565	Al 1.556
Al(2) 1.549	–	–
O(1) 6.909	O 6.952	O 6.963
O(2) 6.948	–	–

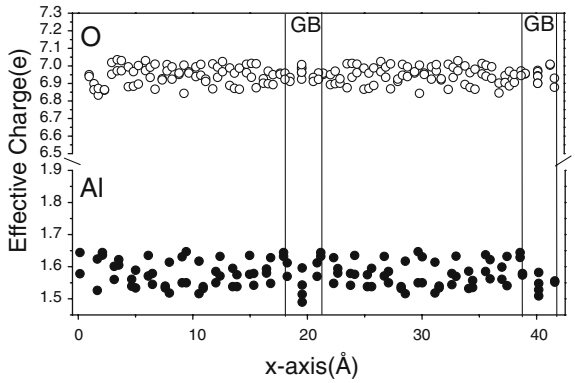

Fig. 2 Calculated effective charges (Q^*) for all the atoms in the Σ37 GB

Table 1 together with the BL and Q^* values. It can be seen that in the GB region, there are both long and short bonds compared to crystalline α-Al_2O_3. These short Al–O bonds have relatively larger BO values and the longer ones have weaker bonds. It has to be reminded that it is the weaker bonds that are responsible for the fracture of the materials under strain [1].

Figure 3 shows the calculated total density of states (TDOS) and partial DOS (PDOS) of Al and O atoms as well as the PDOS of Al(1), Al(2), O(1), and O(2) in the GB region. The PDOS of the bulk atoms are similar to those in the α-Al_2O_3 crystal [13]. The most interesting features are in the PDOS of the GB atoms. The most conspicuous features are the two sharp peaks in the PDOS of the under coordinated O(1) near the top of the valence band (VB) at –0.54 and –1.27 eV, respectively. Careful analysis shows that the upper peak originates from the bonding of O(1) to Al(1), the under coordinated Al in the GB with a BL of 1.839 Å. The lower peak can be traced to the bonding of O(1) with two Al(2) ions with a BL of 1.823 Å. The PDOS of O(2) is very different from O(1) and is somewhat closer to the bulk O ions since they are all 6-fold bonded. The main peak at –4.10 eV is slightly lower than the same peak in the PDOS of the bulk O ions. The rather sharp peak at –9.11 eV is the result of strong bonding between O(2) and Al(2) with a rather short BL of 1.810 Å. The peak locations in the lower O-2s band below –16 eV for O(1) and O(2) basically confirm the explanations for the structures in the PDOS of the upper VB.

The PDOS of Al(1) and Al(2) in the GB region are also very interesting. We focus on the states near the conduction band (CB) edges. There are sharp peaks near the CB edges that intrude into the gap. The lowest ones are at 3.92 eV for Al (1) and 4.02 eV for Al(2). These are the anti-bonding states of the sharp peaks seen in the O(1) PDOS at the top of the VB as

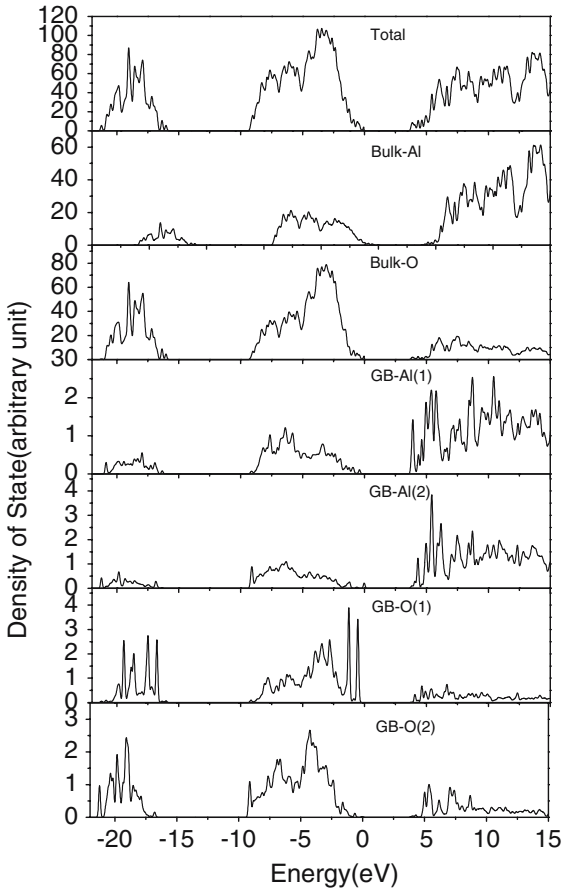

Fig. 3 Calculated total and partial DOS of the Σ37 GB model using the OLCAO method

discussed above. The occurrence of the defect-like structures at the top of the VB (mostly from the O ions) and at the bottom of the CB (mostly from the Al ions) has resulted in the reduction of the LDA gap to 3.90 eV compared to 6.31 eV for the crystalline α-Al_2O_3 using the same OLCAO method [13].

The above results are preliminary since the structure could be further relaxed which may slightly change its electronic structure and bonding. The calculation for the Y-doped Σ37 model is currently in progress and will be reported elsewhere. We anticipate that it will be easier for the larger Y ions to be accommodated at the Σ37 GB because of the larger open spaces in the GB region. Nevertheless, similar calculations on the simpler Σ3 model in the basal plane have been published [1]. Data from theoretical tensile experiments on pure α-Al_2O_3, an undoped Σ3 GB, and a Y-doped Σ3 GB show that Y enhances the interatomic covalent bonding through the participation of Y-4d and Y-3p orbitals [1]. Such results can be used to provide the quantum mechanical explanation for the so-called ''Y-effect''; that the addition of Y to alumina can increase the creep resistance due to the segregation of the Y ions to

the GB region and the increased cohesiveness due to Y addition [27, 34–38]. Similar calculations on a much more complex Σ31 GB model where good experimental data on creep rate using bi-crystal exist have also been attempted [2].

IGF in β-Si_3N_4

Figure 4a shows an IGF model in β-Si_3N_4 with 798 atoms and periodic boundary conditions. The model was initially constructed using molecular dynamics (MD) with repeated quenching from high temperature [4]. The MD relaxed model was then further relaxed using VASP. The difference in energy between the MD relaxed model and the VASP relaxed model is only 47.4 eV or less than 0.06 eV per atom. This indicates that the potential used in the MD simulation is quite accurate because it gives the structure close to the one relaxed by the ab initio method. However, from the stand point of the electronic structures, such fine tuning of the atomic positions by ab initio techniques is important. The calculated DOS of the IGF model shows defect-like structures near the band edges and these defect-like structures are different in the MD relaxed model and the VASP relaxed model, indicating that the electronic states near the gap region are very sensitive to minor structural modifications [4].

It has been known for a long time that the width and the fracture toughness of the IGF depend on the rare earth content of the IGF [38–42]. These rare earth elements are the result of using metal oxides as sintering aids in the high temperature processing of Si_3N_4. To understand the effect of Y-doping in an IGF, we replaced 16 Si atoms by 16 Y atoms in the IGF region of the 798 atom model with simultaneous substitutions of the same number of N ions by O ions to maintain the overall charge neutrality. However, the likely distribution of the Y ions within the IGF is not known. We therefore designed four possible distribution patterns of the 16 Y atoms in the IGF: (1) random distributions of the Y ions across the IGF (2) a distribution with Y ions residing predominately at the interface (3) a graded distribution with more Y ions in the interior of the IGF region (4) a graded distribution with more Y ions at the interface of the IGF and the crystal planes. The four distribution models were then relaxed by VASP. The interface model (2) had the lowest energy and was therefore chosen as the representative model of the Y-doped IGF which is shown in Fig. 4b.

The electronic structure and bonding of the Y-doped IGF were calculated using the OLCAO method. In Fig. 5, we show the calculated DOS and the

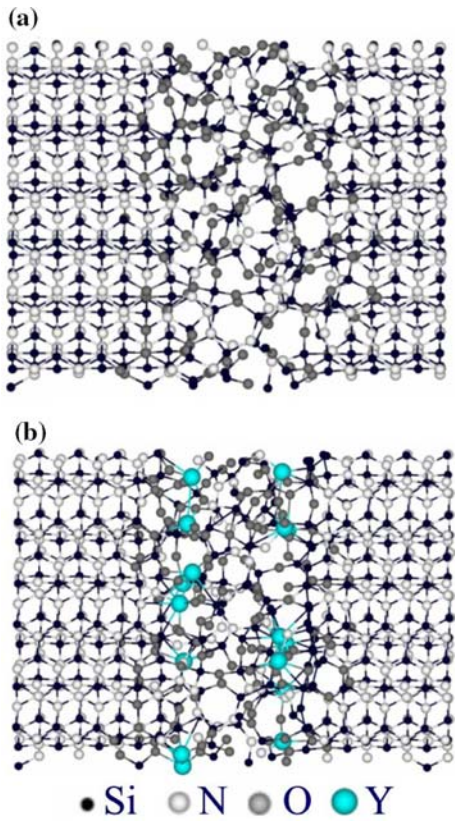

Fig. 4 The periodic structure model of an IGF between basal planes of crystalline β-Si3N4: (**a**) without Y doping (**b**) with Y-doping. The 16 Y ions are in the IGF region close to the interfacial boundaries of the IGF and the crystal

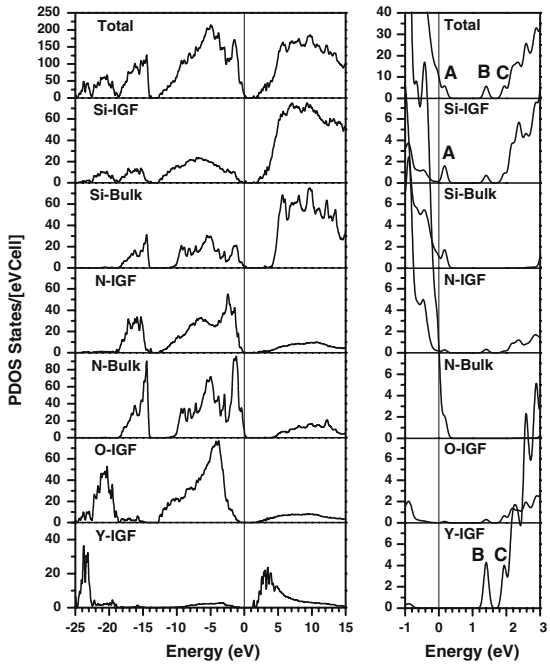

Fig. 5 Calculated DOS and atom-resolved PDOS of the Y-doped IGF

atom-resolved PDOS. The introduction of Y ions and the redistribution of Si, O, and N in the IGF resulted in the reduction of the band gap from 3.2 eV in the undoped case [4] to 2.0 eV in the Y-doped case. The Y states are more pronounced in the energy region below –22 eV (from Y-3p) and near the conduction band (CB) edge (mainly Y-4d). Close inspection of the DOS near the gap region shows the presence of three defect-like structures labeled A, B, and C. State A is an acceptor level 0.09 eV above the VB top. B and C are closer to the CB edge and are respectively 1.31 and 1.76 eV from the top of the VB. Analysis of the wave functions associated with these states shows that A originates from a group of atoms, two under-coordinated Si atoms in the crystalline region near the IGF and another Si atom in IGF close to them. One of the Si atom in the bulk crystal bonds to three N and the other to two N and one O. These under-coordinated Si ions in the bulk region are the result of the initial interphase mixing in the top three layers on the crystal side [4]. These results clearly show that electronic states near the band gap depend very sensitively on the local structure at the IGF and crystalline boundaries. States B and C originate from pairs of close Y ions separated by 3.12 and 3.04 Å, respectively. Also contributing to these states is a near-by Si ion. The presence of these defect-like states will have implications for the application of polycrystalline silicon nitrides in microelectronic devices.

The mechanical and elastic properties of the Y doped and undoped IGF models were studied by theoretical tensile experiments similar to the GB model discussed above. The details of these calculations have been reported elsewhere [5]. In short, under uni-axial strain, the Y-doped IGF shows a very complicated deformation behavior and the doping of Y in the IGF has greatly enhanced the elastic and the mechanical properties of the IGF. This enhancement can be attributed to several factors including the increased covalent bonding of Y which has 3d electrons in the valence shell and 3p electrons in a semi-core level, and the rearrangement of the inter-atomic bonds in the interfacial region.

Connection to continuum level theory

The information obtained from the present atomic level electronic structure calculations may be used to further investigate fundamental issues related to the significance of GBs and IGFs on the overall mechanical behavior of materials. The results of our simulations form a necessary basis for developing a better definition of the relationships between atomistic scales and microscopic scales in ceramics. For example, these results taken together with the knowledge of ceramic morphology and composition could be used to develop mesoscopic scale (nano/micrometer) coarse grained constitutive models through multi-scaling techniques [43, 44]. Mesoscales become important for ceramics due to their unique responses in time and length scale. As mentioned earlier, the first-principle calculations are extremely computationally expensive and not practically feasible at a scale larger than about 2,000 atoms. Therefore, first principle studies may be used to validate and improve empirical potentials used in MD simulations. With these reliable empirical potentials, MD based atomistic simulations can be applied to study mechanical properties (including the desirable temperature effects) of systems of greater scale (≥10,000 atoms) with much greater efficiency. However, ab initio quantum mechanical methods or molecular dynamics (MD) have difficulty in analyzing multi-scalar hierarchical structures (that may have billions of atoms) due to the limitations in terms of the time and length scales that these methods are confined to. Although the classical MD simulations have found wide applications in elucidating complex physical phenomena, the length and time scales that can be modeled using MD are still fairly limited. In recent years, models have been developed that implement MD in localized regions and utilize finite elements everywhere else. However, these models typically run into the confounding problem of widely different fundamental time periods in the two regions, and consequently, have not satisfactorily addressed the bridge between the atomistic and continuum regimes. Therefore, multi-scale methods that incorporate coarse grained constitutive relationships [45, 46], which links the discrete and continuum representations, and may be implemented into finite element or similar analysis tools, offer a powerful simulation technique for multi-scalar hierarchical structures such as ceramics. Simulation techniques that bring together the deep insight of first-principles atomistic simulations and the power of continuum mechanics are expected to have wide application in materials science and engineering.

Concluding remarks

In conclusion, we have shown that large-scale ab initio modeling of complex microstructures in structural ceramics is possible and can provide a wealth of information that is otherwise impossible to obtain. We presented the preliminary results on the electronic

structure for the Σ37 GB and showed the profound effect of under-coordinated atoms in the GB region on the electronic structure and bonding. They introduce defect-like structures near the band gap edges and also reduce the gap. We show that the doping of Y to the grain boundaries of alumina and to the IGF structures in Si_3N_4 can significantly enhance their mechanical and elastic properties. Our calculations also reveal the atomic origin of the electronic states associated with the defect-like structures in the IGF models. Such results cannot be obtained from a classical type of simulations. We further sketch the road map of how to use the information obtained from the ab initio modeling to link them to other simulations at larger length scales. These efforts will be put to test in the near future.

Acknowledgments Work is supported by US Department of Energy under Grant No. DE-FG02–84DR45170 and by NSF Grant No. DMR-00162 in collaboration with NANOAM Project of EU-CODIS (G5RD-CT-2001–00586). This research used resources of NERSC supported by Office of Science of DOE under contract No. DE-AC03–76SF00098.

References

1. Chen J, Rulis P, Xu Y-N, Ouyang L Ching WY (2005) Acta Mater 53:403
2. Buban J, Matsunaga K, Chen J, Shibata N, Ching WY, Yamamoto T, Ikuhara Y (2006) Science 311:212
3. Chen J, Ouyang L, Ching WY (2005) Acta Mater 53:4111
4. Rulis P, Chen J, Ouyang L, Ching WY, Su X-T, Garofalini SH (2005) PhysRev B 71:235317
5. Chen J, Rulis P, Ouyang L, Misra A, Ching WY (2005) Phys Rev Lett 95:256103
6. Hohenberg P, Kohn W (1964) Phys Rev B 136:864
7. Kohn W, Sham LJ (1965) Phys Rev A 140:1131; Sham LJ, Kohn W (1966) Phys Rev 145:561
8. Kresse G, Hafner J (1993) Phys Rev B 47:558
9. Kresse G, Furthmuller J (1996) Comput Mat Sci 6:15
10. Ching WY (1990) J Am Ceram Soc 71(11):3135
11. Ching WY, Xu Y-N (1994) J Am Ceram Soc 77(2):404
12. Huang M-Z, Ouyang L, Ching WY (1999) Phys Rev B 57:3737
13. Xu Y-N, Ching WY (1999) Phys Rev B 59:10530; Ching WY, Xu Y-N (1999) Phys Rev B 59:12815
14. Ching WY, Mo S-D, Ouyang L, Tanaka I, Yoshiya M (2000) Phys Rev B 61:10609
15. Ching WY, Xu Y-N, Ouyang L (2002) Phys Rev B 66:235106
16. Ouyang L, Randaccio L, Rulis P, Kurmaev EZ, Moewes A, Ching WY (2003) J Molec Structures (Theo Chem) 622:221
17. Ouyang L, Ching WY (2004) J Appl Phys 95(12):7918
18. Ching WY, Ouyang L, Yao H-Z, Xu Y-N (2004) Phys Rev B 70:085105
19. Ching WY (2004) J Am Ceram Soc 87(11) 1996 (Feature article)
20. Mulliken RS (1995) J Chem Phys 23:1833
21. Gülgün MA, Putlayev V, Rühle M (1999) J Am Ceram Soc 82(7) 1849; J Am Ceram Soc 82 (1999) 1497
22. Bruley J, Cho J, Chan HM, Harmer MP, Rickman JM (1999) J Am Ceram Soc 82(10):2865
23. Wang CM, Cargill GS, Chan HM, Harmer MP (2000) Acta Mater 48:2579
24. Cho J, Rickman JM, Chan HM, Harmer MP (2000) J Am Ceram Soc 83(2):344
25. Voytovych R, Maclaren I, Gülgün MA, Cannon RM, Rühle M (2002) Acta Mater 50:2453
26. Wang CM, Slade Cargill G, III, Chan HM, Harmer MP (2002) J Am Ceram Soc 85(10):2492
27. Matsunaga K, Nishimura H, Muto H, Yamamoto T, Ikuhara Y (2003) Appl Phys Lett 82:1179
28. Li Y, Wang CM, Chan HM, Rickman JM, Harmer MP, Chabala JM, Gavrilov KL, Levi-Setti R (1999) J Amer Ceram Soc 82:1497
29. Fabris S, Nufer S, Marinopoulos AG, Elsasser C (2002) Phys Rev B 66:155415
30. Marinopoulos AG, Elsässer C (2000) Acta Mater 48:4375
31. Fabris S, Elsässer C (2001) Phys Rev B 64:245117
32. Elsässer C, Marinopoulos AG (2001) Acta Mater 49:2951
33. Fabris S, Elsasser C (2003) Acta Mater 71:51
34. Nakamura A, Shibata N, Morishige N, Matsunaga K, Yamamoto T, Ikuhara Y (2005) J Am Ceram Soc 88:938
35. Matsunaga K, Nishimura H, Hanyu S, Muto H, Yamamoto T, Ikuhara Y (2005) Appl Surf Sci 241:75
36. Matsunaga K, Nishimura H, Saito T, Yamamoto T, Ikuhara Y (2003) Philos Mag 83:4071
37. Nishimura H, Matsunaga K, Saito T, Yamamoto T, Ikuhara Y (2003) J Am Ceram Soc 86:574
38. Hoffmann MJ, Petzow G (1994) Tailoring of Mechanical Properties of Si_3N_4 Ceramics (NATO ASI Series E, Applied Sciences) vol 276, Kluwer Academic, Dordrecht
39. Lange FF, Davis BI, Metcalf MG (1983) J Mater Soc 18:1497
40. Kleebe H-J, et al (1993) J Am Ceram Soc 76:1969
41. Tanaka I, et al (1994) J Am Ceram Soc 77:911
42. Becher PF, et al (2000) Acta Mater 48:4493
43. Liu WK, et al (2004) Comput Methods Appl Mech Engrg 193:1529
44. Gghoniem NM, et al (2003) Philosophical Mag 83:3475
45. Misra A (2004) In: Pietruszczak S, Pande G (eds) Numerical Models in Geomechanics, Balkema A. A., Rotterdam, The Netherlands, p 5
46. Thiagarajan G, Misra A (2004) Intl J Solids Struct 41:2919